PHILOSOPHICAL TRANSACTIONS OF THE ROYAL SOCIETY B BIOLOGICAL SCIENCES

Modelling Mechanically Stable Muscle Architectures

J. L. Van Leeuwen and C. W. Spoor

Phil. Trans. R. Soc. Lond. B 1992 **336**, 275-292
doi: 10.1098/rstb.1992.0061

Modelling mechanically stable muscle architectures

J. L. VAN LEEUWEN[1] AND C. W. SPOOR[2]

[1]*Neuroregulation Group, Department of Physiology, Leiden University, Wassenaarseweg 62, P.O. Box 9604, NL-2300 RC, Leiden, The Netherlands*
[2]*Department of Biomaterials, School of Medicine, Building 55, Leiden University, Rijnsburgerweg 10, NL-2333 AA Leiden, The Netherlands*

CONTENTS

SUMMARY

This paper presents a planar architectural model for an activated skeletal muscle, with mechanical equilibrium throughout the muscle belly. The model can predict the shape of the muscle fibres and tendinous sheets as well as the internal pressure distribution in the central longitudinal plane (perpendicular to the tendinous sheets) of uni- and bipennate muscle bellies. Mechanically stable solutions for muscle architectures were calculated by equating the pressure developed by curved muscle fibres with the pressure under a curved tendinous sheet. The pressure distribution under a tendinous sheet is determined by its tension, its curvature and the tensile stress of the attached muscle fibres. Dissections showed a good resemblance of the architecture of embalmed muscles with those from our simulations. Calculated maximum pressures are in the same order of magnitude as pressure measurements from the literature. Our model predicts that intramuscular blood flow can be blocked during sustained contraction, as several experimental studies have indeed demonstrated. The volume fractions of muscle fibres and interfibre space in the muscle belly were also calculated. The planar models predict a too low volume fraction for the muscle fibres (about 45% for the bipennate models with a straight central aponeurosis, and about 60% for the simulated unipennate muscle). It is discussed how, in a real muscle, this volume problem can be solved by a special three-dimensional arrangement of muscle fibres in combination with varying widths of the tendinous sheets.

1. INTRODUCTION

The force and power output of a muscle-tendon complex (MTC) depends on (i) the activation and mechanical properties of its muscle fibres, (ii) the arrangement of the muscle fibres in the muscle belly (muscle architecture), (iii) the viscoelastic properties of the tendinous sheets and tendons, and (iv) the external loading of the MTC. The present paper deals mainly with the second aspect.

For centuries, researchers have been interested in the functional architecture of skeletal muscles. Some of the classical papers on this topic were by Stensen (1667), Haughton (1873), Benninghoff & Rollhäuser

Phil. Trans. R. Soc. Lond. B (1992) **336,** 275–292
Printed in Great Britain

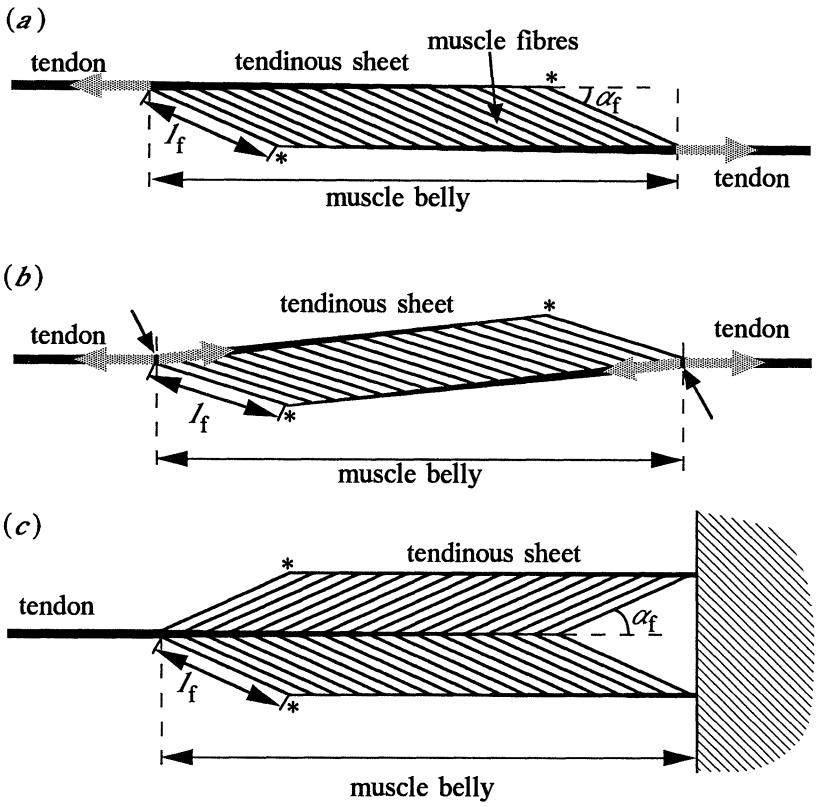

Figure 1. (*a*) Unipennate muscle model with an unexplained torque on the muscle belly, caused by tendon forces (grey arrows) which are not in line. (*b*) Unipennate muscle model with unrealistic angles between tendons and tendinous sheets. Grey arrows depict forces on a cross-section through the connection between tendon and tendinous sheet. Black arrows point to such cross-sections. (*c*) Bipennate model architecture. The asterisks in (*a*), (*b*) and (*c*) are positioned near very unstable regions of the muscle architectures. See § 2 for symbols. Further explanation in the text.

(1952), and Gans & Bock (1965), while Alexander (1969) is a classical account on fish trunk muscles. Recent reviews and models, including dynamic aspects of muscles, were presented by Otten (1988), Zajac (1989), and Van Leeuwen (1992).

Most models of muscle architecture are either unipennate or bipennate. All unipennate models violate fundamental laws of classical mechanics. Some models have an unbalanced torque on the muscle belly, caused by parallel tendons on either side of the muscle belly which are not in line (figure 1*a*; used, for example, by Zajac (1989)). Other unipennate models have tendons which are in line (used, for example, by Huijing & Woittiez (1984) and Otten (1985, 1988)). Those models, however, have an unexplained angle between tendon and tendinous sheet (figure 1*b*). A cross-section through the connection between tendon and tendinous sheet would not be in equilibrium owing to the different directions of the forces acting on it. In conclusion, the unipennate models of figures 1*a*, *b* are mechanically unstable and therefore unrealistic. The symmetry of bipennate muscle models (figure 1*c*) largely avoids the described problems of the unipennate models (used, for example, by Alexander (1983), Spoor *et al.* (1989) and Van Leeuwen (1992)).

All architectural models of figure 1 have straight muscle fibres throughout the muscle belly. However, curved fibres and tendinous sheets are needed to create mechanical stability. For instance, unstable situations occur near the positions of the asterisks in figure 1, where the superficial muscle fibres make a considerable angle with the tendinous sheet. At corresponding positions in real muscles (observed by dissection), the attachment angles are zero or close to zero, while the fibres and tendinous sheets are curved.

The intramuscular pressure distribution has to be considered for the calculation of mechanically stable muscle architectures. In discussing how pressure could be produced in the human gastrocnemius, Hill (1948, p. 521) pointed out that the curved muscle fibres exert a pressure inwards when they contract (i.e. exert force), depending on their tension and radius of curvature. Similarly, Otten (1988) argued that the intramuscular pressure can be built up by layers of curved muscle fibres under tension. He made also calculations for the pressure under a tendinous sheet with attached muscle fibres. Otten's implementation of this useful concept in a unipennate muscle model was, however, still hampered with mechanical flaws (cf. Otten 1988, figure 14): (i) the instability problem associated with the angle between tendon and tendinous sheet was still present; (ii) the chosen shape of the tendinous sheets and the chosen muscle-fibre arrangement are incompatible, caused by a separate treatment of the contributions of muscle fibres and tendinous sheets to the intramuscular pressure. This leads

to an incorrect estimate of the intramuscular pressure distribution. The high-pressure centres, suggested to be present under each of the tendinous sheets, are covered with only a relatively thin layer of curved muscle fibres which would not be able to balance this pressure.

The present paper describes how mechanically stable solutions for muscle architectures can be obtained by equating the pressure developed by curved muscle fibres with the pressure under a curved tendinous sheet. In this approach, only a limited set of boundary conditions is prescribed. Muscle geometry is numerically generated using the clearly defined physical principle of mechanical equilibrium. Furthermore, account is taken of the space between neighbouring muscle fibres. Model results will be qualitatively compared with architectural features of some leg muscles of man.

2. SYMBOLS AND DEFINITIONS

Symbols denoted with * represent normalized quantities.

A_{fib}	total cross-section of all muscle fibres in a muscle belly.
c_f; c_{fb}; c_{fq}	curvature of a muscle fibre ($c_f = 1/R_f$); idem, but at right boundary of muscle belly (figure 2*c*); idem, but as $s = q$.
c_s; c_{sb}; c_{sq}	curvature of a tendinous sheet (allowed to vary along the sheet; $c_s = 1/R_s$); idem, but at right boundary of muscle (figure 2*c*); idem, but at $s = q$.
F_{fib}; F_{fibt}; F_{mus}	muscle-fibre force; part of fibre force transmitted to muscle force; muscle force.
F_{ph}	longitudinal component of internal pressure force at right boundary (figure 2*d*).
F_{pts}; F_{ptsh}	force exerted at right boundary of peripheral tendinous sheet; idem, but longitudinal component only (figure 2*d*).
F_{pu}	pressure force at boundary of unipennate model (figure 7*b*, *c*).
l_f; l_{fb}	muscle-fibre length; length of muscle fibre at right boundary of muscle belly.
l_{pts}	total length of peripheral tendinous sheet.
MTC	muscle-tendon complex.
p; p_b	intramuscular pressure; idem but at right boundary of muscle.
p_{max}; p^*_{max}	maximum intramuscular presssure; idem but normalized with respect to the maximum muscle-fibre stress.
p_{trq}	pressure component under tendinous sheet at $s = q$, due to the tensile stress in the tendinous sheet in the transverse direction.
p_q	pressure under tendinous sheet at $s = q$.
q	point on peripheral tendinous sheet.
r_f	coordinate in a direction perpendicular to the direction of a muscle fibre.
R_f	radius of curvature of a muscle fibre (assumed to be constant along the fibre).
R_s	radius of curvature of a tendinous sheet (allowed to vary along the sheet).
R_{sq}	radius of curvature of a tendinous sheet at $s = q$.
s	position along peripheral tendinous sheet (curvilinear coordinate).
T_{csq}	tensile force in central tendinous sheet (corresponding to position q at peripheral sheet; equation 8).
T_{sq}	local tensile force at $s = q$ in peripheral tendinous sheet.
u	exponent in equation (12).
V_{fib}; V^*_{fib}	total fibre space in muscle belly; volume fraction of muscle fibres with respect to total muscle volume ($V^*_{fib} = V_{fib}/V_{mus}$).
V^*_{fibloc}	local volume fraction of muscle fibres.
V_{fq}	fibre space from $s = 0$ to $s = q$.
V_{iq}	interfibre space in muscle belly from $s = 0$ to $s = q$.
V_{mus}	total volume of muscle belly.
V_{tq}	total volume from $s = 0$ to $s = q$ (i.e. $V_{fq} + V_{iq}$) (figure 2*f*).
w	width of considered muscle slice, tendinous sheet element or muscle fibre.
α_f	attachment angle between central tendinous sheet and muscle fibre (figure 2*c*).
α_{fb}	angle of attachment between central tendinous sheet and muscle fibres at right boundary of muscle belly (figure 2*c*, *f*).
β_f; β_{fb}; β_{fq}	attachment angle between peripheral tendinous sheet and muscle fibre (figure 2*b*, *c*); idem, but at right boundary of muscle belly (figure 2*c*); idem, but at $s = q$.
γ_f	effective pennation angle of a muscle fibre (equation 10).
δ; δ_b	angle between peripheral and central tendinous sheet at the attachment position of a particular muscle fibre (figure 2*c*); idem but at right boundary of muscle.
Δp	intramuscular pressure difference.
Δr_f	thickness of a muscle fibre.
σ_f; σ_{fb}; σ_{fq}	tensile stress exerted by a muscle fibre; idem, but at right boundary of muscle belly; idem, but at $s = q$.

3. MATERIALS

Some specimens of the gastrocnemius and soleus muscles, dissected from embalmed human cadavers,

PHILOSOPHICAL TRANSACTIONS OF THE ROYAL SOCIETY B BIOLOGICAL SCIENCES

were used to check (qualitatively) some of the predictions of the architectural models. The embalming fluid contained per litre: 30 g chloral hydrate, 50 g sal Carolineum facticium (i.e. 2% K_2SO_4, 18% NaCl, 36% $NaHCO_3$, 44% $Na_2SO_4 \cdot H_2O$), 75 cm^3 formalin (36% by mass), 50 cm^3 ethanol (96% by volume), 10 cm^3 glycerol, and 10 cm^3 phenol. The legs were fixed with extended knees and the feet in plantar flexion. One medial gastrocnemius muscle was cut perpendicular to the tendinous sheet so as to expose the central longitudinal plane, which was subsequently photographed. The pictures were used for a qualitative comparison of architectural data like tendinous sheet length and curvature, and muscle-fibre lengths and curvatures with model simulations. Quantitative comparisons were not made as these require an as yet unavailable specialized experimental set up for *in vivo* measurement of these parameters in activated muscles.

4. THE MODEL

Most calculations in this paper apply to a planar bipennate muscle model (figure 2*c*), with two curved peripheral tendinous sheets and one (straight) centrally positioned tendinous sheet. The symmetry of this model simplifies the required numerical computations. In fact, the middle longitudinal muscle slice (perpendicular to the tendinous sheets) of width w (w is small compared to the muscle width) is considered. This slice is assumed to be in mechanical equilibrium with the neighbouring muscle parts at both sides. The central tendinous sheet is connected at the left side to an in-line tendon. At the right side, the two peripheral sheets are connected under an angle δ_b to a tendon in line with the left tendon. As shown in figure 2*c* in exaggerated form, the two peripheral tendons do not exactly meet. In the simulations (figures 4, 5, 6), however, the distance between them is made negligibly small. The parameter values for the right side will be denoted as boundary conditions. The shaded area at the right boundary does not contain muscle fibres and may be considered as a fluid-filled (incompressible) chamber. This chamber is pressurized as a result of tensile muscle-fibre stress (see below). In the simulations, the chamber is made very small compared to the size of the muscle belly. The developed model can be readily extended (albeit with increased numerical complexity) to other architectures and more realistic three-dimensional shapes. A unipennate simulation will be discussed in § 5*d* (figure 7). Three-dimensional effects will be addressed qualitatively in § 6*b*.

Let us first consider the pressure gradient (figure 2*a*) generated by activated muscle fibres with radius of curvature R_f, curvature c_f ($= 1/R_f$), tensile stress σ_f and thickness Δr_f. The pressure difference Δp between the concave side and the convex side of the fibre is given by

$$\Delta p = (\sigma_f \Delta r_f)/R_f. \quad (1)$$

Putting equation (1) in infinitesimal form, the pressure gradient can be obtained:

$$\partial p/\partial r_f = \sigma_f/R_f = \sigma_f c_f. \quad (2)$$

We will now discuss how the pressure in the muscle belly is built up along the peripheral tendinous sheet by successive layers of curved muscle fibres. The mechanical influence of the connective and adipose tissue surrounding the muscle fibres and fibre bundles will be neglected. Purslow (1989) modelled the load-sarcomere length curve of the perimysium and showed good agreement with passive elastic properties of the muscle. He concluded that the role of the perimysial collagen network is to prevent over-stretching of the muscle-fibre bundles above a sarcomere length of 3.6 μm. Most likely, the endomysium works in a similar fashion. Therefore, in an activated muscle working around optimum sarcomere length, the contribution of the endo- and perimysium to force output can generally be neglected.

Furthermore, it will be assumed that each muscle fibre has a constant cross-sectional area, a constant tensile stress, and a constant curvature along its length. Of course, these properties are allowed to vary among the muscle fibres. The functional explanation for a constant cross-section and a constant tensile stress is that fibres should be of equal strength along their length to avoid as much as possible one part doing work on the other (Otten 1988). Histological studies show that muscle fibres taper only where they attach to collagen fibres, just before their connections to the tendinous sheets. Analogously to hydrodynamic studies, we will call the thin layer with tapering muscle fibres under the tendinous sheet the boundary layer. In the sequel, it will be assumed that the boundary layer has zero thickness. We hope to deal with the mechanical aspects of this layer in a future paper. A consequence of the constant curvature assumption (in our two-dimensional approach) is that pressure contours run parallel to the muscle fibres. Apart from reasons of simplicity, we chose for a constant muscle-fibre curvature, because it seems favourable for a muscle fibre if it operates with a relatively small pressure gradient along its length. Furthermore, it seems likely that the muscle would change shape so as to minimize the pressure gradient, if a significant gradient along the muscle fibres would be present. This assumption agrees with our model representation of the interfibre space between neighbouring muscle fibres with a constant pressure over the volume if the muscle belly is in static equilibrium (see below and figure 2*e*). Some change in curvature along muscle fibres may be observed in real muscles. As will be explained in § 6*b*, this change may actually help to minimize the pressure gradient along the fibres, owing to the special three-dimensional arrangement of the fibres.

The tendinous sheets are assumed to have no bending stiffness. Let s be a curvilinear coordinate describing the distance along the peripheral tendinous sheet ($s = 0$ at the left end, figure 2*c*), let β_f be the attachment angle of a muscle fibre to the peripheral tendinous sheet (in reality, β_f is the angle at which the muscle fibres penetrate the boundary layer), and let α_f be the attachment angle at the central tendinous sheet. If a muscle fibre is attached over a distance ds onto the sheet, then the muscle-fibre thickness is

PHILOSOPHICAL TRANSACTIONS OF THE ROYAL SOCIETY B BIOLOGICAL SCIENCES

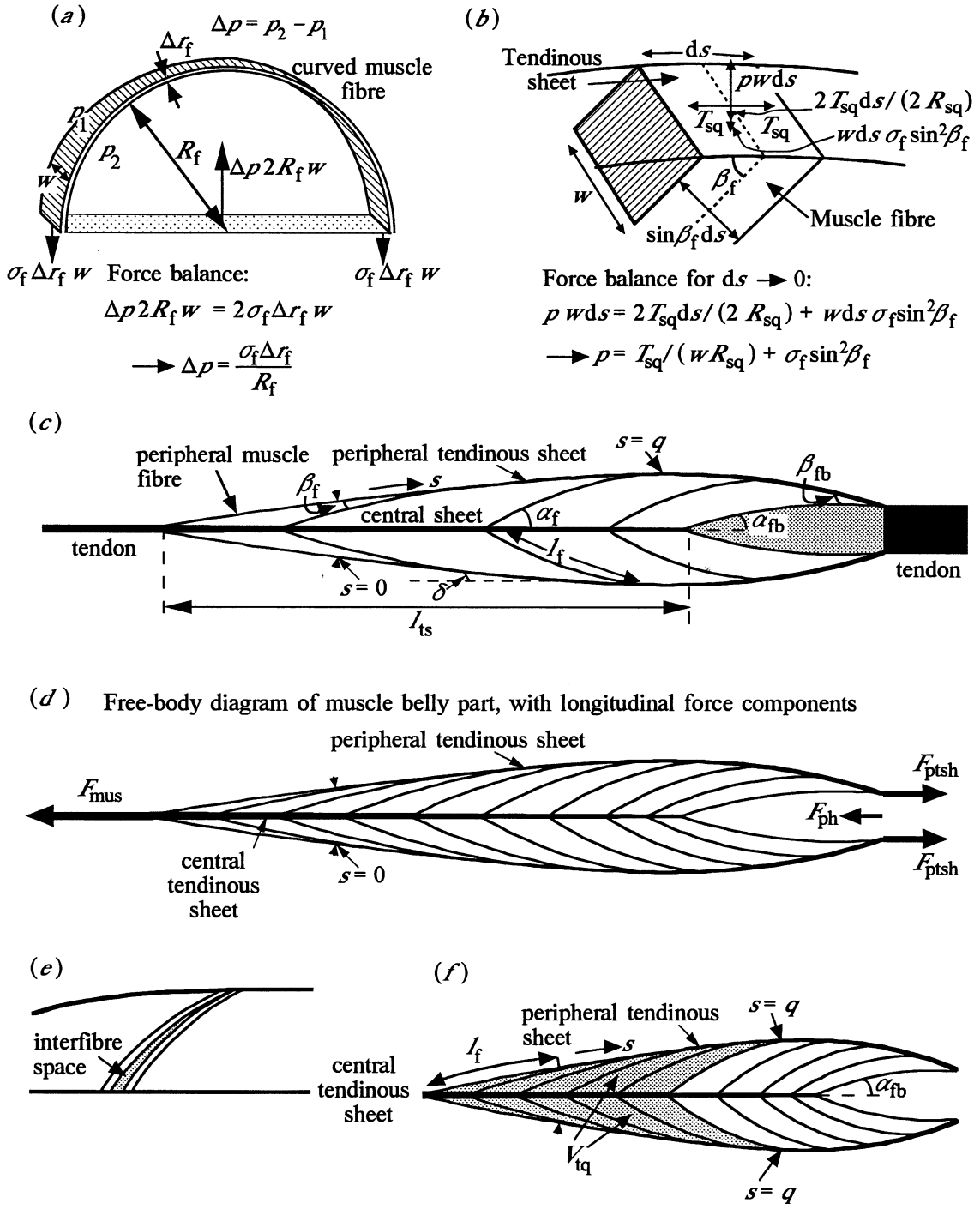

Figure 2. (*a*) Diagram illustrating how pressure is generated by pulling of a curved muscle fibre. (*b*) Diagram illustrating how the pressure under a tendinous sheet can be calculated (equation 4). The influence of the transverse tensile stress in the sheet is not shown for reasons of simplicity. (*c*) Diagram illustrating some parameters of a bipennate muscle model as explained in the text. Note that the attachment angles change by different amounts along the peripheral and central tendinous sheets. (*d*) Free-body diagram of a part of a muscle belly. (*e*) Illustration of the interfibre space between subsequent muscle fibres of different orientation and curvature. Only one half of the muscle belly is shown. (*f*) The shaded area depicts the volume V_{tq}. Arrow heads in (*c*), (*d*), and (*f*) point to the transitions between tendinous sheet and peripheral muscle fibre. See § 2 for symbols.

$\sin\beta_f\,ds$. Generally, β_f varies along the tendinous sheet. The internal pressure generated by the muscle fibres at a point q along s is given by (using equation 2, see also figure 2*c*)

$$p_q = \int_0^q \sigma_f c_f \sin\beta_f\,ds. \qquad (3)$$

A pressure gradient is present across the peripheral tendinous sheet: outside the sheet the ambient pressure acts and under the sheet the intramuscular pressure acts as described by equation (3). The pressure difference at a point q can be expressed (figure 2*b*) in terms of (i) the longitudinal tensile force

T_{sq} in the tendinous sheet, the local sheet radius of curvature R_{sq} (both T_{sq} and R_{sq} vary along the sheet) and the width w of the sheet, (ii) a similar term in the transverse direction, and (iii) the local muscle-fibre stress σ_{fq} and the local attachment angle β_{fq}

$$p_q = T_{sq}/(R_{sq}w) + p_{trq} + \sigma_{fq} \sin^2 \beta_{fq}. \quad (4)$$

The first term on the right-hand side is equivalent to equation (1). The second term is similar to the first term. Its components need not be specified in our two-dimensional approach. The third term is needed to account for the contribution of the tensile muscle-fibre stress to the pressure (the squared sine is needed because (i) the muscle-fibre force is proportional to fibre thickness, which equals the attachment distance along the sheet times $\sin \beta_{fq}$, and (ii) the force component perpendicular to the sheet has to be considered which equals muscle-fibre force times $\sin \beta_{fq}$). The tensile force (along s) at position q in the peripheral tendinous sheet can be calculated from the muscle-fibre stress along the sheet and the attachment angle β_f along the sheet

$$T_{sq} = w \int_0^q \sigma_f \cos \beta_f \sin \beta_f \, ds. \quad (5)$$

The $\cos \beta_f$ is required because the component of the muscle-fibre force parallel to the sheet is considered. The sine term is again needed to obtain the fibre thickness from the attachment distance. Using equation (5), equation (4) can be rewritten as

$$p_q = \frac{1}{R_{sq}} \int_0^q \sigma_f \cos \beta_f \sin \beta_f \, ds + p_{trq} + \sigma_{fq} \sin^2 \beta_{fq}. \quad (6)$$

Now, the muscle pressure p_b at the right boundary can be derived from the boundary values of the tensile force in the tendinous sheet per unit width, the sheet curvature c_{sb}, and the muscle-fibre stress σ_{fb}, once the attachment angle β_f and tensile stress σ_f of the muscle fibres as well as the total length of the peripheral tendinous sheet l_{pts} are prescribed (see below and figure 2*c*).

The pressure distribution can be strongly influenced by shape changes in the muscle belly (affecting fibre attachment angles and curvatures of muscle fibres and tendinous sheets, see § 5). Of course, the muscle-fibre stress distribution is also a dominant component for the pressure distribution. The maximum muscle pressure depends on the tensile fibre stress and the attachment angles, but not on the size of the muscle. The size independence of the maximum pressure, also noted by Hill (1948) and Otten (1988), can be understood as follows. The radii of curvature of the muscle fibres and tendinous sheets increase in proportion to muscle size. Therefore, the pressure gradient will be inversely proportional to muscle size (equation 2). The effect this has on the maximum pressure, however, is cancelled by the muscle length (and tendinous sheet length, equation 3) which is proportional to muscle size.

At every position along the peripheral tendinous sheet (i.e. for every s), the pressure generated by the muscle fibres (equation 3) should be equal to the pressure calculated from tendinous sheet curvature and tensile force, and muscle-fibre stress (equation 6). Hence,

$$\int_0^q \sigma_f c_f \sin \beta_f \, ds = \frac{1}{R_{sq}} \int_0^q \sigma_f \cos \beta_f \sin \beta_f \, ds + p_{trq} + \sigma_{fq} \sin^2 \beta_{fq}. \quad (7a)$$

The local radius of curvature of the tendinous sheet is obtained by rearranging equation (7*a*):

$$R_{sq} = \int_0^q \sigma_f \cos \beta_f \sin \beta_f \, ds \Big/ \left(\int_0^q \sigma_f c_f \sin \beta_f \, ds - p_{trq} - \sigma_{fq} \sin^2 \beta_{fq} \right). \quad (7b)$$

Quite importantly, equation (7) shows how a tendinous sheet shape can be calculated which is compatible with the pressure built up by successive layers of curved and activated muscle fibres.

Analogous to equation (5), the tensile force in the central tendinous sheet (corresponding to position q at the peripheral sheet) can be calculated as

$$T_{csq} = F_{mus} - 2w \int_0^q \sigma_f \cos \alpha_f \sin \beta_f \, ds, \quad (8)$$

where F_{mus} is the total muscle force (figure 2*d*). For convenience, parameter s is used as integrand here because, along the central sheet, interfibre tissue is assumed to be present between the muscle fibres (see below and figure 2*e*). For a particular muscle fibre, s has the same value at both tendinous sheets. The total muscle force can be calculated from (figure 2*d*):

$$F_{mus} = 2 F_{ptsh} - F_{ph} = 2 F_{pts} \cos \delta_b - F_{ph} = 2 w \cos \delta_b \int_0^{l_{pts}} \sigma_f \cos \beta_f \sin \beta_f \, ds - F_{ph}, \quad (9)$$

where F_{pts} is the tensile force at the right boundary in the peripheral sheet, F_{ptsh} ($= F_{pts} \cos \delta_b$) is the longitudinal component of this force, F_{ph} is the longitudinal component of the pressure force on the muscle belly at the boundary, and δ_b is the angle between peripheral sheet and tendon at the boundary.

A single muscle fibre mostly attaches with different angles on the peripheral and central tendinous sheets (or, better, penetrates the boundary layers at different angles). The question now arises to what extent this influences the force transmission of the muscle fibres. In a bipennate muscle, the conventional rule that the force transmission to the aponeurosis equals fibre force times the cosine of the attachment angle can be applied to both the central aponeurosis and the peripheral aponeuroses. Consider a curved muscle fibre attaching with angle α_f to the central aponeurosis in a bipennate muscle (like those depicted in figures 2*c*, 4*a* and 5*a*). The muscle-fibre force F_f is directly transmitted to the central aponeurosis with component $F_f \cos \alpha_f$, and with component $F_f \cos \beta_f$ to the peripheral aponeurosis. Because $\beta_f < \alpha_f$ for most of the fibres (see figures 4 and 5), the sum of the tensile forces

PHILOSOPHICAL TRANSACTIONS OF THE ROYAL SOCIETY B BIOLOGICAL SCIENCES

built up in the two peripheral sheets is greater than the tensile force built up in the central sheet. This difference, however, is exactly compensated by the angle of attachment of the peripheral tendinous sheet with the tendon (neglecting F_{ph}, because the peripheral sheets almost meet at the right boundary). For the considered muscle belly, the forces in the longitudinal direction cancel (see free-body diagram of figure 2*d* and equation 9).

A single, well-defined, pennation angle for a muscle belly does not exist. In fact, the pennation-angle concept is likely to have biased many measurements of muscle architecture in the past. It is perhaps most appropriate to define the effective pennation angle γ_f of a muscle fibre in relation to the transmission of fibre force to muscle belly force:

$$\gamma_f = \arccos\,(F_{fibt}/F_{fib}), \tag{10}$$

where F_{fib} is the fibre force, and F_{fibt} is the part of the fibre force being eventually contributed to the muscle force. In the somewhat idealistic bipennate muscle belly, γ_f is equal to α_f. In general, however, γ_f need not be equal to one of the attachment angles.

The above set of equations allows to generate numerically a wide range of mechanically stable muscle architectures. Only a subset of this range is expected to correspond to architectures found in nature. Quite often, muscle-fibre length varies only slightly throughout the muscle belly (Spoor *et al.* 1991). In this paper, we will use an 'ideal' distribution of muscle-fibre length defined by

$$l_f = l_{fb} \cos \alpha_f / \cos \alpha_{fb}. \tag{11}$$

This distribution is loosely based on the assumption that, in an infinitesimal muscle shortening, all muscle fibres should contract by the same relative amount so that work by them is produced in proportion to fibre volume (Benninghoff & Rollhäuser 1952). Strictly speaking, the equality of fibre work is only fulfilled by the length distribution in a model with straight muscle fibres and a translation of the peripheral tendinous sheet parallel to the central tendinous sheet (both sheets assumed to be inextensible). As a result of geometric limitations (more than one muscle fibre cannot be present at the same place), this distribution cannot always be realized in our muscle model (see figures 4*e* and 5*e*). Benninghoff & Rollhäuser (1952) have correctly argued that the actual range of muscle shortening is a better criterion to predict the relationship between fibre length and pennation angle. Here, we deal with muscle bellies in static equilibrium. A particular choice of muscle shortening would anyhow be arbitrary in this theoretical study. Therefore, we have chosen a length distribution corresponding to an infinitesimal shortening. Furthermore, one should not be too strict about the concept of equal specific work output for all muscle fibres, since, in one muscle belly, different muscle-fibre types are generally present. For instance, in the m. levator operculi of the perch a slow type is present with very long actin filaments and a fast type with much shorter actin filaments (Akster 1981). The differences in actin filament length point to different excursions of the muscle fibres. Longer actin filaments guarantee a smaller sensitivity of power output to muscle-fibre strain (Van Leeuwen 1991).

The attachment angle β_f was (tentatively) described as a power function of s:

$$\beta_f = \beta_{fb} \{s/l_{pts}\}^u. \tag{12}$$

Now, the volume distribution of muscle fibres and interfibre space within the muscle belly will be considered. The volume of the muscle fibres attached to both sides of the central tendinous sheet is given by

$$V_{fq} = 2w \int_0^q l_f \sin \beta_f \, ds. \tag{13}$$

Neighbouring muscle fibres in the muscle belly have slightly different radii of curvature and attachment angles. Therefore, some space is present between the fibres (figure 2*e*). In calculating this space, it will be assumed that the fibres have no space in between at the peripheral sheet. Morphologically, one may think that the interfibre space is filled with connective tissue, adipose tissue, blood vessels or nerves. The interfibre space V_{iq} associated with the attached fibres from $s = 0$ to $s = q$ can be obtained by subtracting V_{fq} from the total volume V_{tq} (figure 2*f*) enclosed by the first muscle fibre, the peripheral tendinous sheet up to q, the muscle fibre at q, and the corresponding structures in the opposite muscle half:

$$V_{iq} = V_{tq} - V_{fq}. \tag{14}$$

Although some blood may be squeezed out of the muscle belly during intramuscular pressure development, it seems a good approximation if both V_{fq} and V_{iq} are kept constant in simulations of muscle belly length change and force development. Let V_{fib} be the total muscle-fibre volume and let V_{mus} be the total volume of the muscle belly. Then, the global fractional fibre space V^*_{fib} is calculated as V_{fib}/V_{mus}. Apart from the global fraction, a local volume fraction of the fibres (V^*_{fibloc}) was calculated as half the volume of two neighbouring fibres divided by this same volume plus the enclosed interfibre volume.

To calculate the shape of a mechanically stable slice of a skeletal muscle belly, the following strategy was applied.

1. Prescribe the attachment angle along the peripheral sheet $\beta_f(s)$ using equation (12) and prescribe the tensile stress distribution in the muscle fibres.
2. For simplicity, the muscle belly is 'mathematically clamped' at the right boundary of the muscle (figure 2*c*). The clamping (boundary) conditions are prescribed, i.e. tendinous sheet orientation and curvature, muscle-fibre attachment angle, length, and curvature.
3. Initially, give a rough estimate of the tendinous sheet length. Adjust the tendinous sheet length in subsequent iterations so as to converge to the required solution.
4. Starting from the clamping side, calculate (i) the curvature $c_f(s)$ for successive muscle fibres such that the length condition of equation (11) is fulfilled (if this would result in overlap of muscle fibres, the nearest

PHILOSOPHICAL TRANSACTIONS OF THE ROYAL SOCIETY B BIOLOGICAL SCIENCES

fibre curvature and length without overlap is taken), and (ii) the corresponding tendinous sheet curvature R_s using equation (7*b*).

5. Step (4) is stopped and the process restarted at step (3) if either the gradient in muscle-fibre curvature falls below or above certain limits, fibres would have to penetrate each other, or the calculated pressure is not close enough to zero at the distal fibre boundary. If none of these ill conditions are met, then the calculated architecture is accepted as a mechanically stable solution.

6. Calculate the muscle volume, fibre volume, interfibre volume and volume fractions.

With the prescribed peripheral attachment angle and the prescribed relationship between (central) pennation angle and fibre length, a unique solution corresponds to a particular set of clamping conditions.

Apart from the above description for a bipennate model, we also simulated unipennate architectures. We limited our analysis to muscle bellies which are curved as a whole. Examples are both heads of the human m. gastrocnemius, whose concave sides face the m. soleus and tibia. As a result, the tendons at both sides of the muscle belly are not in line. If the muscle produces force, it presses against underlying tissues. Thus, ambient forces play an important role in the mechanical equilibrium of the muscle belly, whereas, in the modelled bipennate architecture, equilibrium of the central tendinous sheet is ensured by the equality of force amplitudes at both sides. Therefore, virtually the same computational scheme could be applied for this unipennate muscle architecture.

The above model was implemented in a computer programme, allowing to simulate force and pressure development by the muscle belly. The model can also be used to study effects of different architectures on the mechanical performance. Dynamic properties of a simplified version of this model with straight muscle fibres of equal length were discussed by Van Leeuwen (1992).

5. RESULTS AND DISCUSSION

Before discussing various simulations of muscle architectures, we consider the influence of the exponent u (equation 12) on the nature of the attachment of the peripheral muscle on the left tip of the peripheral tendinous sheet. Figure 3*a* shows the numerically approximated limit value of c_{sq}/c_{fq} (i.e. the ratio of sheet curvature and fibre curvature at the tip) for $q \rightarrow 0$ as a function of u (calculated from equation 7*b*; values of various parameters in figure legend). It was assumed that $p_{trq} = 0$ (see equation 7*b*). Figure 3*b* shows the same limit value against $d\beta_f/ds$ (the gradient of the attachment angle at the tip). A consideration of the gradient is interesting since the conclusions are of a more general nature than those obtained with exponent u. The curvature of the tip of the tendinous sheet is about equal to the peripheral fibre curvature ($c_{sq} \approx c_{fq}$) for low values of $d\beta_f/ds$ (i.e. u greater than about 1.3). For increasing values of $d\beta_f/ds$, the tip curvature drops with an increasing rate (the fibre curvature is kept fixed along each curve), while a discontinuity in sheet curvature and peripheral fibre curvature is present. The curvature ratio c_{sq}/c_{fq} depends on the peripheral fibre curvature as indicated in figure 3. The range with negative c_{sq}/c_{fq} at the aponeurosis tip represents situations with an upward curving sheet at the tip (a situation which is not often found in nature). In our bipennate simulations, we used curvature ratios which were close to 1, except in figure 6*g*, where a negative ratio was applied. If p_{trq}/p_q increases at the tip, then the sheet curvature will decrease compared to the curvature of the peripheral muscle fibre.

The present model covers an infinite set of solutions for mechanically stable muscle architectures. Here, we will discuss two different solutions for the bipennate muscle model. Both solutions have a peripheral tendinous sheet curvature at the tip which is almost equal to the peripheral muscle-fibre curvature. Furthermore, a limited survey of possible bipennate muscle shapes will be presented. Finally, a unipennate simulation will be discussed, loosely based on the architecture of the human medial gastrocnemius muscle. For simplicity, equal stresses for all muscle fibres will be used in all simulations of this paper. Variable fibre stresses can, however, in principle be handled with our theory.

(*a*) *Bipennate model with moderate attachment angles of muscle fibres*

(i) *Starting conditions*

In most muscles at optimum length for force output, muscle-fibre attachment angles are below 25°. In a fully contracted soleus muscle, angles may be as large as 60° (cf. Spoor *et al.* 1991; Wickiewicz *et al.* 1983). A maximum value of only 7.5° for β_f can already be considered as moderate, especially as it may be accompanied with a maximum value for α_f of about 16° (figure 4*d*). Figure 4 illustrates the results of a simulation of a bipennate muscle model with moderate angles of attachment of the muscle fibres (parameter values are given in table 1). At the right muscle boundary, the peripheral tendinous sheets were chosen to have an angle δ_b of $-11.5°$ with the central aponeurosis (one of the clamping conditions). The influence of the transverse tensile stress in the peripheral tendinous sheet was neglected (i.e. $p_{trq} = 0$ in equation 7).

(ii) *Muscle-fibre arrangement*

Figure 4*a* shows how the muscle fibres are arranged in the muscle belly. Except for a small part at the right side of the muscle belly, α_f is larger than β_f owing to fibre curvature and peripheral sheet orientation (figure 4*c*, *d*). This leads to a concentration of interfibre space around the central aponeurosis. The calculated total volume fraction of the muscles fibres is only about 0.43 for this particular architecture. This unrealistically low value is a direct consequence of (i) the two-dimensional approach, and (ii) the different sheet orientations. In § 6*b*, it will be discussed how, in

PHILOSOPHICAL TRANSACTIONS OF THE ROYAL SOCIETY B BIOLOGICAL SCIENCES

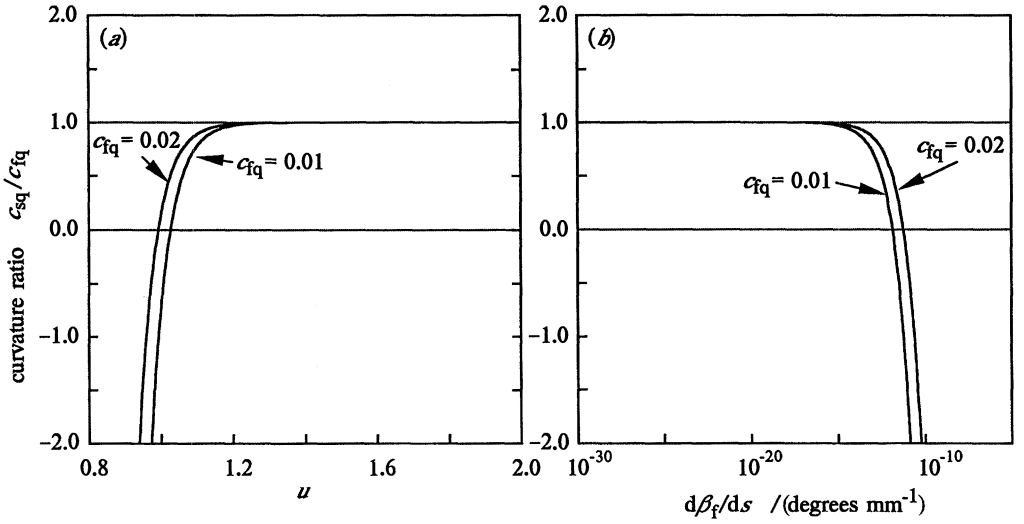

Figure 3. The numerically approximated limit value of c_{sq}/c_{fq} for $q \rightarrow 0$ (i.e. the ratio of the tip curvature of the peripheral aponeurosis over the peripheral muscle-fibre curvature), calculated from equation (7*b*), against (*a*) the exponent u (see equation 12) and (*b*) the gradient of the attachment angle $d\beta_f/ds$ along a logarithmic scale. The two curves in each plot represent different values of the peripheral fibre curvature c_{fq} (in mm^{-1}) as indicated. The gradients of fibre curvature and tensile stress were chosen as $dc_f/ds = 0.0005$ and $d\sigma_f/ds = 0$, respectively.

a real muscle, this problem may be solved. Figure 4*e* shows that the local muscle-fibre fraction increases from about 0 at the tip (left side) of the peripheral tendinous sheet to about 0.91 close to the attachment at the right side. A rapid change in the fraction is observed where the calculated and ideal muscle-fibre length meet at $s \approx 28$ mm.

(iii) *The peripheral tendinous sheet*

The curvature of the peripheral tendinous sheet decreases rapidly from the left-hand tip, goes through a local minimum at $s \approx 1$ mm, rises again up to the global maximum at $s \approx 26$ mm, and then drops towards the boundary value at the right side (figure 4*c*). Muscle-fibre length varies only slightly along the muscle belly (figure 4*e*). A minimum is found for $s \approx 19$ mm. Only over a small distance at the right side, the ideal muscle-fibre length cannot be met owing to fibre-overlap problems. The calculated fibre length is only slightly longer than the ideal length.

(iv) *Intramuscular pressure*

Figure 4*b* shows pressure contours (relative to the maximum pressure) in the muscle belly. The maximum pressure, located at the right boundary of the muscle, is about 7.7 kPa. The pressure increases monotonically from the left to the right side, whereas the pressure gradient (dp/ds) increases from the peripheral muscle fibres (left side) towards the muscle centre, and finally drops towards the right boundary (figure 4*f*, see also the varying widths between the pressure contours in figure 4*b*). The pressure distribution can be understood (using equation 3) from (i) the increasing muscle-fibre curvature along the peripheral tendinous sheet up to $s \approx 22$ mm, followed by a final drop towards the right boundary (figure 4*c*), and (ii) the increasing attachment angle β_f towards the right boundary (figure 4*d*). Close to the right boundary, the negative effect of the drop in fibre curvature on the pressure gradient just overcompensates the positive effect of the increase in β_f.

(*b*) *Bipennate model with large attachment angles of muscle fibres*

Figure 5 illustrates a simulation of a muscle belly with large attachment angles (parameter values in table 1). The boundary values of fibre curvature and the peripheral attachment angle were set to twice the values of figure 4. Compared with figure 4, the following differences may be noted.

1. On average, the peripheral tendinous sheet curvature is considerably higher. A higher boundary curvature was needed to generate a tendinous sheet length of comparable magnitude to figure 4. A local maximum of the sheet curvature is found at $s \approx 25$ mm.

2. Muscle-fibre curvatures are about doubled along the peripheral tendinous sheets (compare figures 4*c* and 5*c*).

3. The internal pressure reaches much higher values (p_{max} is about 31.5 kPa, about a factor of four higher than in figure 4), in spite of a slightly shorter muscle belly length and equal stresses of the muscle fibres. The quadrupled pressure is caused by the (roughly) doubled attachment angles (leading to an almost doubled total thickness of the muscle fibres, i.e. almost twice the amount of muscle is present along the aponeurosis) in combination with the (roughly) doubled fibre curvatures (cf. equations 1 and 3).

4. Not surprisingly, the attachment angles with the central aponeurosis are about doubled (compare the α_f curves in figures 4*d* and 5*d*).

5. The length variation of the muscle fibres along the muscle belly is larger (figure 5*e*), which corres-

PHILOSOPHICAL TRANSACTIONS OF THE ROYAL SOCIETY B BIOLOGICAL SCIENCES

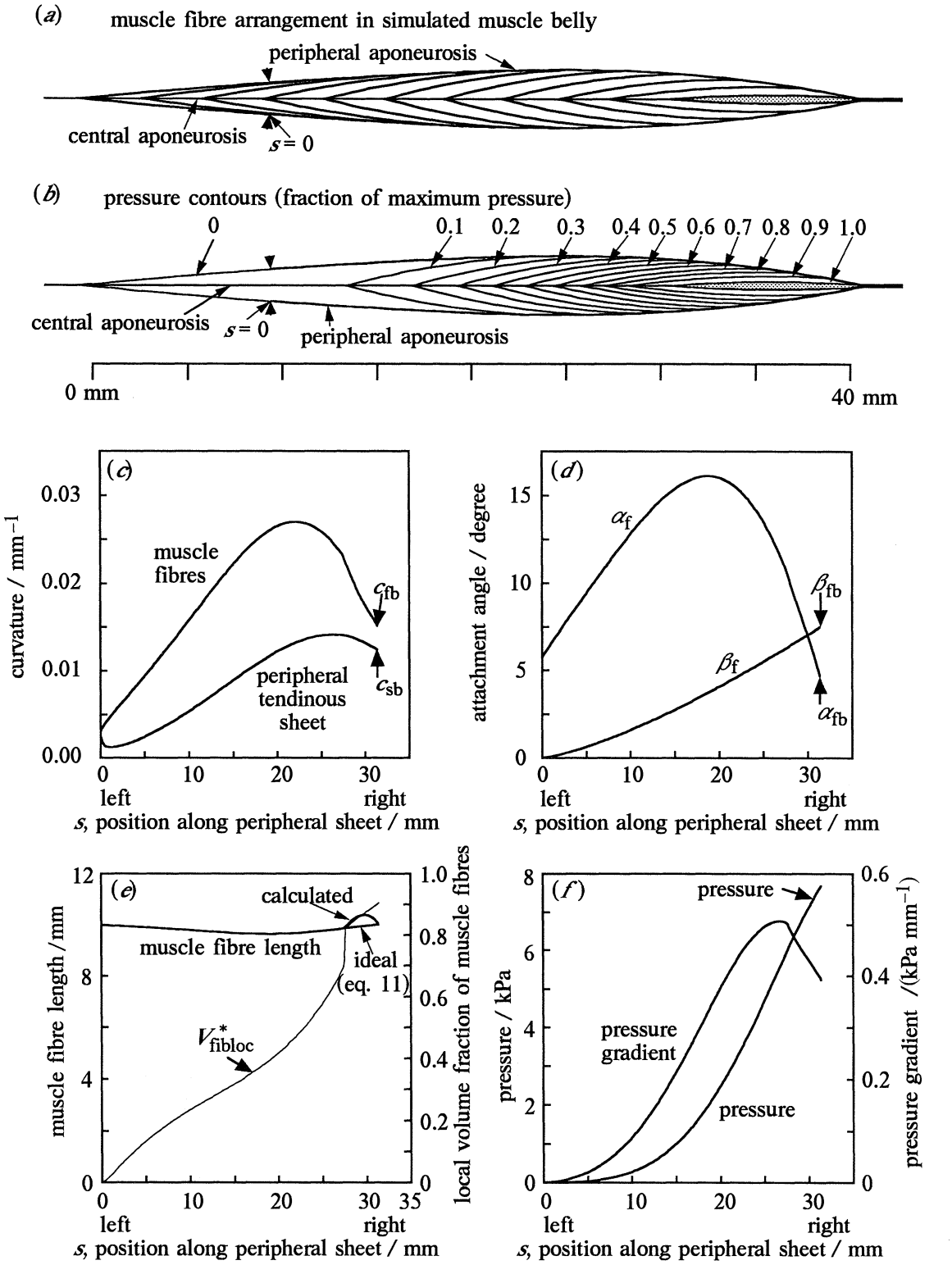

Figure 4. Illustration of the results of a simulation of a bipennate muscle architecture, with 300 muscle fibres used in numerical evaluation. Values of input and output parameters are given in table 1. (*a*) Muscle-fibre arrangement. At each side of the central aponeurosis, 11 fibres are shown, chosen at regular intervals along the peripheral sheets. Arrow heads point to the transitions between tendinous sheet and peripheral muscle fibre. (*b*) Illustration of intramuscular pressure distribution in muscle belly. Contours show values of pressure in fractions of maximum pressure. (*c*) Muscle-fibre curvature c_f and peripheral sheet curvature c_s as a function of the position along the peripheral tendinous sheet s. (*d*) Attachment angles β_f and α_f as a function of s. (*e*) Actual and ideal muscle-fibre lengths as a function of s (normal curves). Local volume fraction of muscle fibres V^*_{fibloc} as a function of s (thin curve). (*f*) Intramuscular pressure and pressure gradient dp/ds as a function of s. Further explanation is given in the text.

Table 1. *Values of input and output parameters of figures 4–6*

(The tensile stress of the muscle fibres (σ_f) was set to 200 kPa for all muscle fibres in all simulations. Furthermore, the muscle-fibre length at the right boundary (l_{fb}) was chosen to be 10 mm, while u (equation 12) was set to 1.35, except for figure 6*g* with $u = 0.8$. The transverse tensile stress in the aponeurosis was neglected in all simulations, except again in figure 6*g*, where the contribution of this stress component to the internal pressure was defined to vary linearly from 0% of the muscle-fibre pressure (equation 3) at the right-hand side of the peripheral sheet to 65% at the left side. Other parameter values (per unit width where applicable) are given below.)

		figure numbers						
symbol	unit	6*a*	4 and 6*b*	6*c*	6*d*	5 and 6*e*	6*f*	6*g*
input:								
c_{fb}	m^{-1}	15.0	15.0	15.0	30.0	30.0	30.0	30.0
c_{sb}	m^{-1}	9.52	12.35	12.76	23.81	26.32	27.06	29.89
β_{fb}	°	7.5	7.5	7.5	15.0	15.0	15.0	15.0
δ_b	°	−11.5	−11.5	−11.5	−23.0	−23.0	−23.0	−23.0
output:								
V_{mus}	mm^2	52.62	79.49	99.04	108.31	141.23	176.91	181.24
V^*_{fib}		0.384	0.434	0.467	0.435	0.463	0.495	0.506
A_{fib}	mm	2.046	3.497	4.698	5.011	6.978	9.373	9.832
l_{pts}	mm	18.39	31.43	42.23	22.61	31.49	42.29	34.01
F_{mus}	(mN mm^{-1})	398.8	681.9	916.1	902.6	1257.8	1690.3	1768.8
F_{pts}	(mN mm^{-1})	203.8	348.9	467.9	493.1	686.7	922.4	965.5
F_{ph}	(mN mm^{-1})	0.6	0.8	1.0	5.1	6.5	7.9	8.7
p_{max}	kPa	5.35	7.71	9.37	25.14	31.47	38.36	42.25
p^*_{max}		0.0267	0.0385	0.0468	0.1257	0.1574	0.1918	0.2113

ponds to the stronger variation in α_f (cf. equation 11). The difference between the ideal and the actual muscle-fibre length at the right side is now more pronounced.

This comparison illustrates the prediction of § 4 that the intramuscular pressure depends strongly on the architecture of the muscle. This will be further exemplified in § 6*c*. The calculated total volume fraction of the muscle fibres is only about 0.46 for this particular architecture, which is again unrealistically low (but see our discussion in § 6*b*). The local fibre fraction (figure 5*e*) shows a similar variation as that of figure 4*e*.

(*c*) *Some examples of stable bipennate architectures*

Figure 6 shows some examples of fibre arrangements of simulated muscle architectures. An overview of values of input and output parameters is given in table 1. Figures 6*a*, *c* are variations on the muscle belly of figure 4 (also depicted in figure 6*b*). All input parameters are kept constant in these three simulations, except for the boundary condition of the peripheral tendinous sheet curvature (c_{sb}). The simulations show that only slight changes in the value of c_{sb} result in quite large changes in muscle belly length. It may also be observed that the relative position of the greatest vertical width of the muscle belly shifts towards the left with a relatively shorter peripheral tendinous sheet length. A shorter muscle belly length (with about the same muscle-fibre lengths and curvatures) gives a lower maximum intramuscular pressure (note that this is accompanied with a change in muscle shape).

Similarly, figures 6*d*, *f* are variations on the muscle belly of figure 5 (also depicted in figure 6*e*), with comparable trends, but with much higher pressures than in figures 6*a–c* owing to the larger cross-sectional areas of the muscle fibres and the stronger muscle-fibre curvatures. The long muscle belly with the large attachment angles of figure 6*f* gives the highest maximum pressure (about 38 kPa with a tensile fibre stress of 200 kPa; normalized pressure: 0.19). The muscle belly of figure 6*a* generates (with the same muscle-fibre stress) a p_{max} of only 5.35 kPa, a more than sevenfold reduction.

For the simulation of figure 6*g*, the parameter u was given a value of only 0.8, leading to, on average, higher attachment angles β_f (equation 12). Furthermore, the contribution of the transverse tensile stress along the peripheral sheets to the internal pressure (p_{trq} in equations 4 and 7) was defined to vary linearly from 0% of the muscle-fibre pressure (equation 3) at the right side to 65% at the left side. The highest influence was defined near the aponeurosis tip since here the longitudinal tensile force is low, whereas, in dissections, transverse sheet curvatures can be found to be quite significant. Compared with the other muscle bellies of figure 6, the parameter changes lead to: (i) a negative peripheral sheet curvature at the left side ($s < 7.5$ mm, see plot in figure 6*g*); (ii) a decreasing muscle-fibre curvature from the sheet tip at $s = 0$ mm to $s \approx 7.5$ mm; and (iii) a more 'bluntly nosed' muscle belly. The maximum pressure of about 42 kPa is slightly higher than the value of the longer muscle belly of figure 6*f*, owing to stronger fibre curvatures at the left-hand side and a higher cross-sectional area of the muscle fibres.

It is repeated here that the intramuscular pressure

PHILOSOPHICAL TRANSACTIONS OF THE ROYAL SOCIETY B BIOLOGICAL SCIENCES

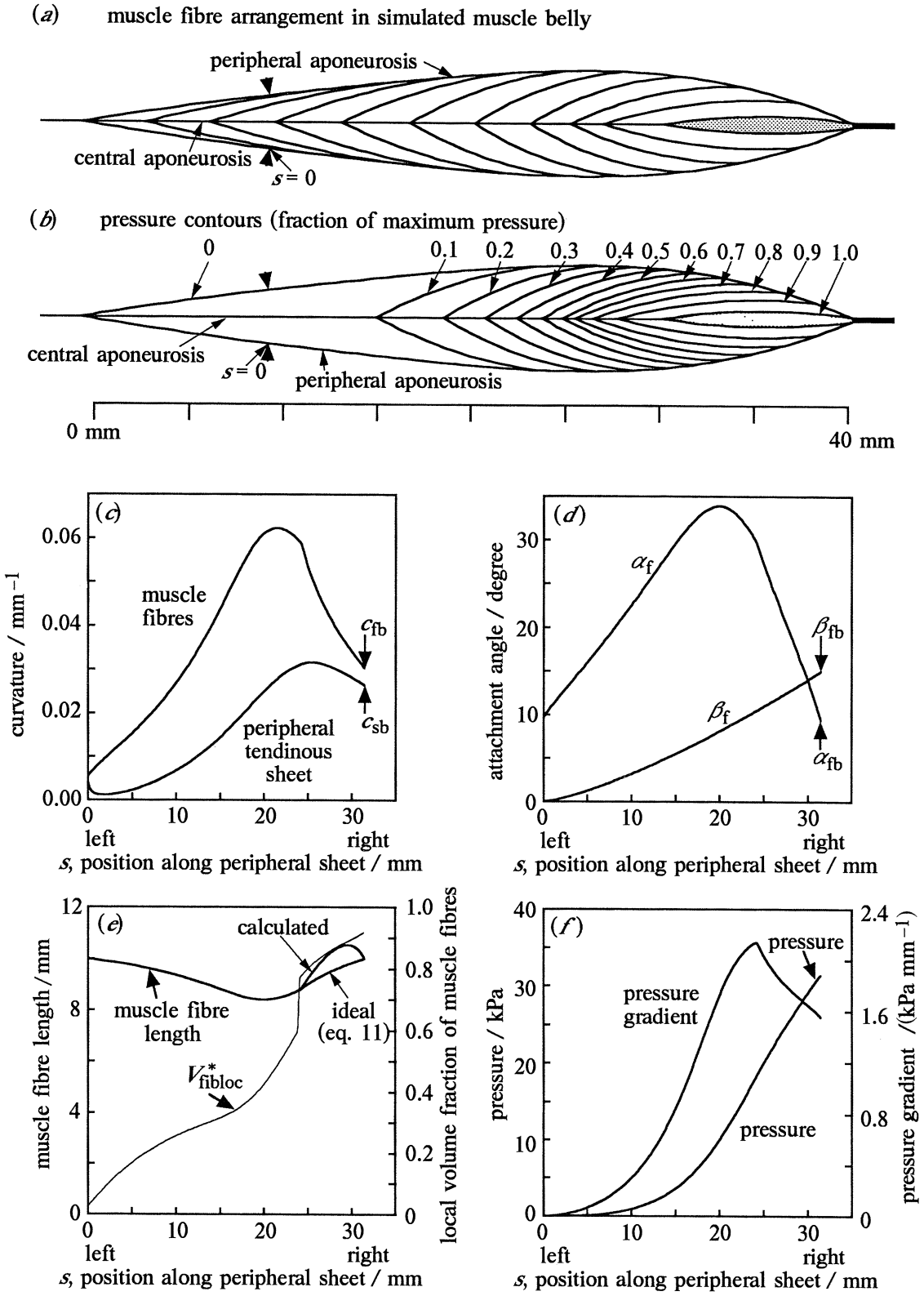

Figure 5. Illustration of the results of a simulation of a bipennate muscle architecture, similarly arranged as in figure 4, but with other values of input and output parameters (see table 1), leading to a more highly pennated muscle belly. See text for further explanation.

and force equilibrium are size independent (if the shape is constant), so that the muscle bellies can be enlarged or reduced to almost any particular size without an effect on the mechanical stability.

(*d*) *Unipennate model based on medial gastrocnemius muscle*

As a whole, the muscle belly of the unipennate

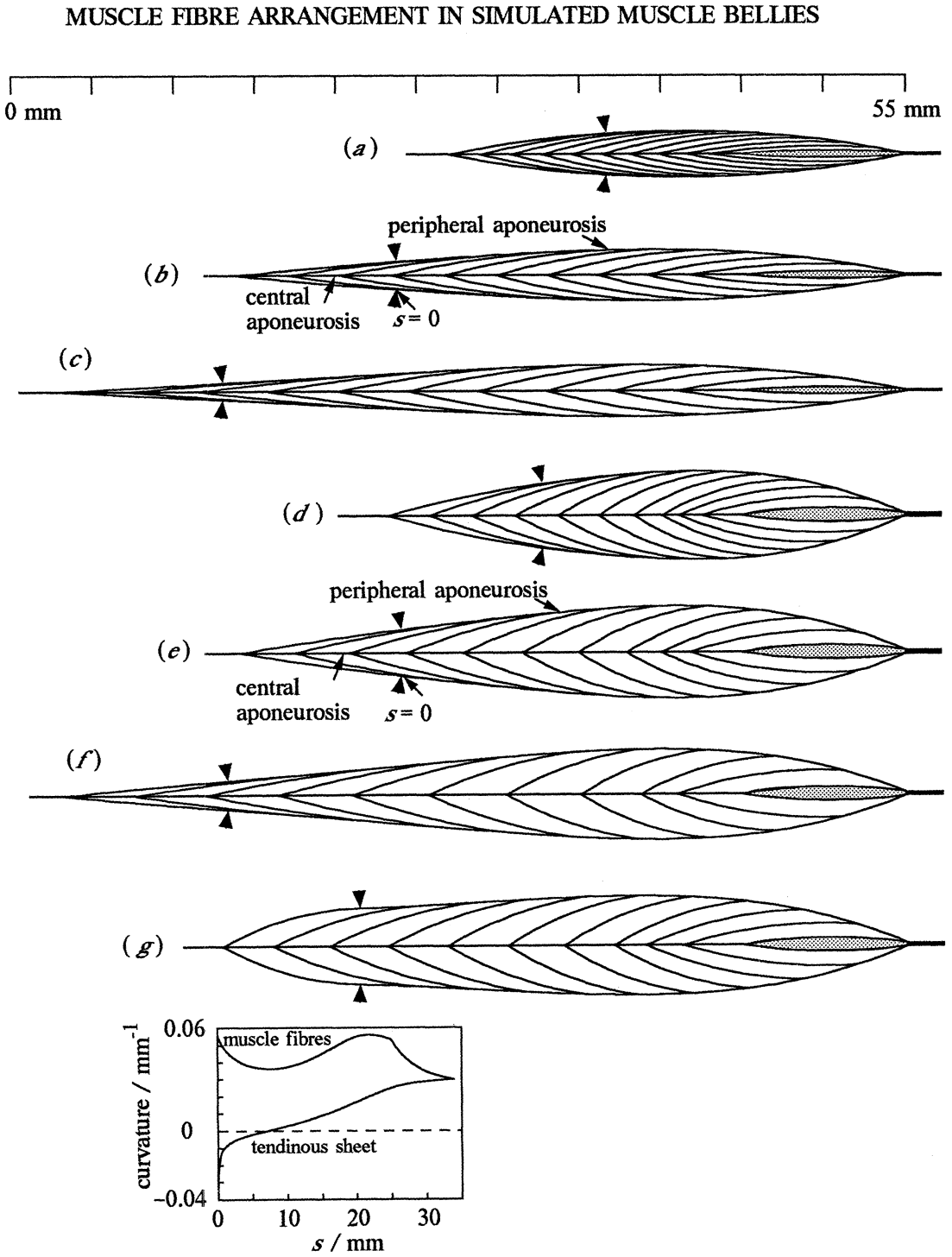

Figure 6. Seven examples of calculated mechanically stable muscle architectures. Muscle belly (*b*) is equal to that of figure 4; (*a*) and (*c*) are variations on (*b*). Muscle belly (*e*) is equal to that of figure 5. (*d*) and (*f*) are variations on (*e*). The muscle architecture in (*g*) is quite different from the other simulations owing to a lower value of exponent *u* (equation 12) and a contribution of the transverse tensile stress in the peripheral tendinous sheets to the force balance. The graph in (*g*) shows the curvatures of muscle fibres and peripheral sheets. Note the difference with figures 4*c* and 5*c*. Arrow heads point to the transitions between tendinous sheet and peripheral muscle fibre. Values of input and output parameters are given in table 1. See text for further explanation.

gastrocnemius medialis (GM) is curved (figure 7*a*), with the concave side facing the tibia. Ambient forces play an important role in the mechanical equilibrium of the muscle belly (see bottom of § 4). Owing to the curved tendinous sheets in the GM, the difference in attachment angle of the fibres at both sheets is expected to be somewhat smaller in the GM than in a comparable bipennate model with a straight central tendinous sheet. Figure 7*b* shows the fibre arrangement of a simulated unipennate muscle belly which is

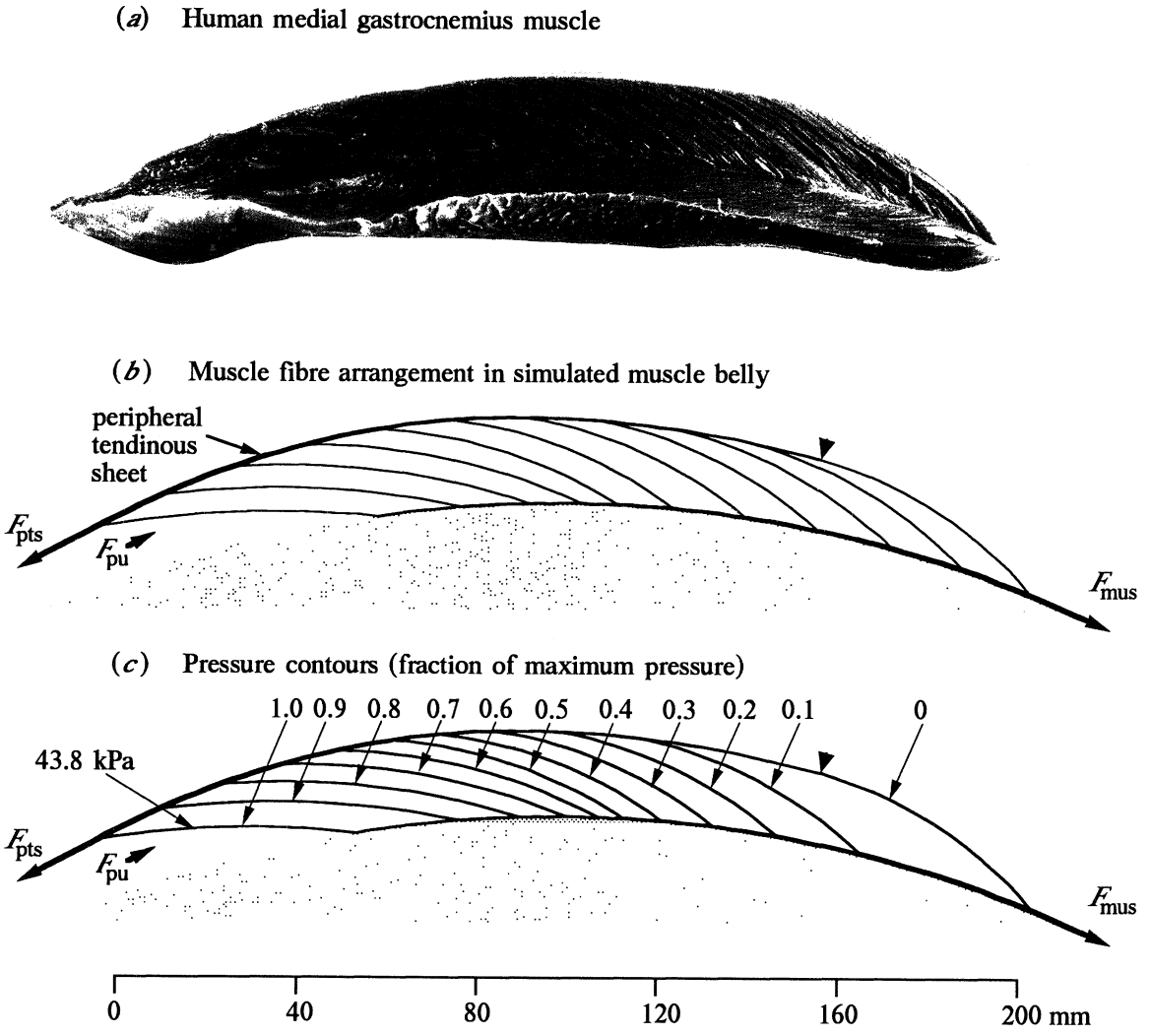

Figure 7. Comparison between human medial gastrocnemius and unipennate simulation. (*a*) Dissected gastrocnemius so as to expose the central longitudinal plane. (*b*) Muscle-fibre arrangement of simulation of mechanically stable unipennate muscle belly. (*c*) Intramuscular pressure contours as a fraction of the maximum pressure (43.8 kPa) of the same simulation. The shaded areas in (*b*) and (*c*) depict the boundary against which the muscle belly presses. Arrow heads point to the transitions between tendinous sheet and peripheral muscle fibre. The scale refers to all illustrations. Some parameter values are as follows (per unit width where applicable): $c_{fb} = 5.10\ m^{-1}$; $c_{sb} = 4.23\ m^{-1}$; curvature of lower sheet $= 3.57\ m^{-1}$; $\beta_{fb} = 18.5°$; $\sigma_f = 200$ kPa; $u = 0.85$; $V_{mus} = 2909.2\ mm^2$; $V^*_{fib} = 0.601$; $A_{fib} = 28.71$ mm; $l_{pts} = 166.0$ mm; $F_{mus} = 5201.5$ mN mm^{-1}; $F_{pts} = 5587.5$ mN mm^{-1}; $p_{max} = 43.79$ kPa; $p^*_{max} = 0.219$. The contribution of the transverse tensile stress along the upper sheet to the internal pressure, p_{trq}, was defined to vary linearly from 0% of the muscle-fibre pressure (equation 3) at the left side to 20% at the right side. See § 2 for symbols. Further explanation in the text.

loosely based on the GM (parameter values are listed in the figure legend; note that clamping is now at the left-hand side). The curvature of the lower sheet was prescribed and kept constant along its length. The overall similarity between the dissected and the simulated architecture is striking, although no special attempt was made to optimize the parameters for this purpose. The left-hand side of the simulated muscle belly is most problematic. Deviations from the ideal fibre length distribution do again occur, since we did not allow the muscle fibres to cross each other. This, in fact, influences the composition of the whole muscle belly. In the real muscle, this problem does not occur since the neighbouring fibres can run in slightly different planes and can bend also in the transverse direction (see also § 6*b*). To simulate the relatively blunt ending of the muscle belly at the right side, we found it essential to use a relatively low value of u (i.e. 0.85, see equation 12) and to include a contribution of the transverse tensile stress along the upper sheet to the internal pressure (p_{trq} was defined to vary linearly from 0% of the muscle-fibre pressure (equation 3) at the left side to 20% at the right side). Figure 7*c* shows the pressure distribution in the simulated muscle, using a uniform muscle-fibre stress of 200 kPa. The maximum pressure of 43.8 kPa and the total fibre fraction of 0.6 are the highest simulated values of this paper.

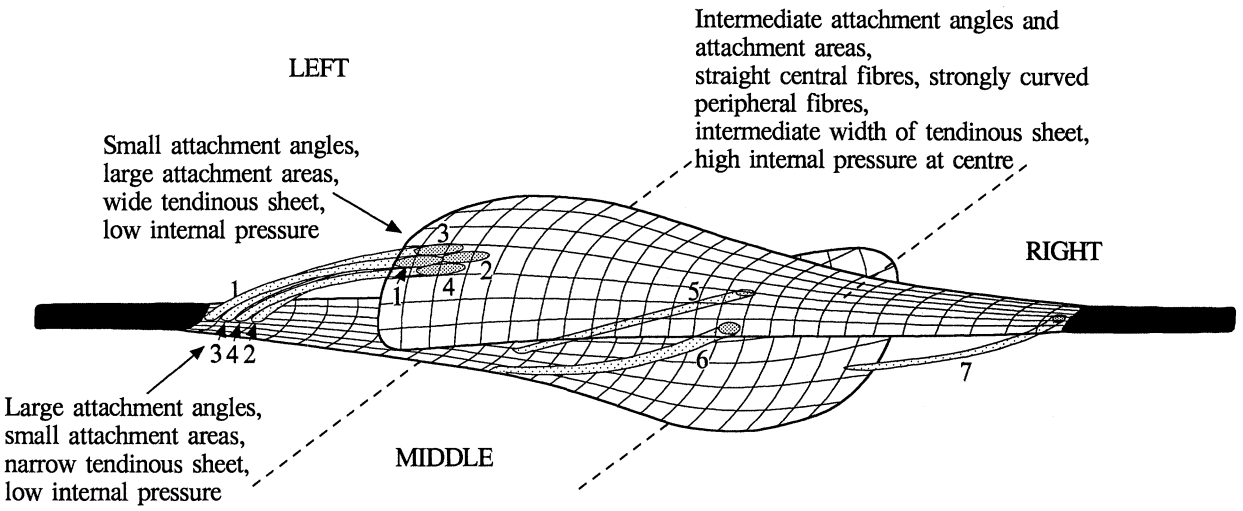

Figure 8. Diagram of a unipennate muscle with in-line tendons (black). The upper tendinous sheet is made transparent for muscle-fibre bundles. Only a few muscle-fibre bundles (numbered 1 to 7) are shown (stippled). Muscle-fibre bundle attachment areas are shown also (heavily stippled). Muscle-fibre bundles 3 and 4 are positioned between bundles 1 and 2 at the lower tendinous sheet so as to obtain an optimal filling of the muscle belly. The central muscle-fibre bundle 5 is straight, whereas the peripheral bundle 6 is strongly curved (this is not very clear owing to the chosen viewpoint). Further explanation in the text.

6. GENERAL DISCUSSION

(*a*) *Comparisons between model predictions and muscle architectures*

Several times in this paper, we refer to a good (qualitative) resemblance between model predictions and muscle architecture observed from dissections. The tensile stresses in a muscle at 'rest' (i.e. not activated and not stretched or compressed) are minimal. An embalmed muscle is likely to have an 'unnatural' stress distribution. The model is designed for situations where the tensile muscle-fibre stress is high compared with the peri- and endomysial stress. So, strictly speaking, the model would not be suitable to predict muscle shapes for the above two possibilities. Nevertheless, it can be argued that a muscle should minimize its deformation from its resting configuration to its stress situation (with a given length of the muscle-tendon complex) since this minimizes internal energy losses. (Of course, the shapes cannot be the same in both situations since tendinous sheets and tendons are stretched by force producing muscle fibres.) We therefore think that several architectural features of the active muscle are already present (at least qualitatively) in a muscle at rest or, alternatively, in an embalmed specimen. Thus, a qualitative comparison between dissections and model results seems to be allowed. This is supported by the good correspondence between our unipennate simulation and the dissected medial gastrocnemius muscle.

(*b*) *Three-dimensional effects*

Using a diagram of a unipennate muscle with in-line tendons (figure 8), we will now discuss some three-dimensional effects. The volume fraction of the fibres was too low in our two-dimensional simulations as compared with a real muscle. The muscle-fibre curvatures and orientations, required for the demands of mechanical stability and the relationship between pennation angle and muscle-fibre length (equation 11), do not allow a close enough fit of neighbouring muscle fibres. The greater attachment angles at the central sheet compared to the peripheral sheet are associated with (owing to the constant cross-sectional area of the fibres) a smaller area of muscle-fibre attachment. In a three-dimensional muscle-fibre arrangement, this problem can easily be solved by allowing neighbouring muscle fibres from both sides (fibre bundles 3 and 4 in figure 8) to penetrate into the spaces between the series of longitudinally arranged (from left to right) muscle fibres (fibre bundles 1 and 2 in figure 8). In this arrangement, the muscle fibres run from a relatively wide tendinous sheet to a much narrower tendinous sheet at the opposite side (left and right side of muscle belly in figure 8). The relative difference in width will generally be most conspicuous close to the attachments to the tendons at both sides of the muscle belly (i.e. the positions with the greatest differences in attachment angles). Thus, to allow an optimal filling of the muscle belly with muscle fibres, tendinous sheets should converge in width from the free edge to their connection with the tendon. This arrangement allows also a 'smooth' transition from tendinous sheet to tendon. The local muscle-fibre volume fractions as shown in figures 4*e* and 5*e* indicate the required width of the central sheet relative to the peripheral sheets (in a three-dimensional arrangement with an optimal filling of muscle fibres).

Dissections of skeletal muscles support these predictions. The described fibre crossing can be observed if one cuts the tendinous sheet in the longitudinal direction, followed by a gentle pulling of both halves

PHILOSOPHICAL TRANSACTIONS OF THE ROYAL SOCIETY B BIOLOGICAL SCIENCES

of the sheet away from the slit. A consequence of the three-dimensional fibre crossing is that, in the central longitudinal plane, relatively more muscle tissue is present at the side with the smallest tendon width. This would result in a larger pressure gradient along this side (as compared with the opposite side), if muscle fibres would have a constant curvature along their length. As a result, a significant pressure gradient would be present along the muscle fibres. This pressure gradient could be avoided if the muscle-fibre curvature decreases from the 'wide' tendinous sheet to the opposite 'narrow' sheet. Therefore, in three-dimensional modelling, a variable fibre curvature should be included. It would be interesting to verify experimentally the predictions of fibre curvature.

Woittiez *et al.* (1984) proposed a unipennate three-dimensional model for the muscle belly. The tendinous sheets were chosen to be kite shaped (with opposite orientation), which roughly corresponds to the shape found in the m. gastrocnemius medialis of the rat and which leads to considerably different insertion areas for individual muscle fibres at both sheets. The chosen tendinous sheet shape corresponds to our prediction for an optimal fibre filling. However, their other (unrealistic) assumptions of straight fibres and straight tendinous sheets would require only small differences in attachment areas because the attachment angles are about equal at both sheets. Hence, these last assumptions are in conflict with the tendinous sheet shapes.

The simulation of a planar unipennate muscle belly (roughly resembling the GM, figure 7) showed that a somewhat higher volume fraction of the muscle fibres was present than in the simulated bipennate muscles of figure 6. This is correlated with, on average, a relatively smaller difference in attachment angle of the muscle fibres into both tendinous sheets in the unipennate architecture (due to the curved tendinous sheet at the concave side).

If pressure p acts in a particular point in a muscle belly, then fibre curvature and arrangement should be such that p is generated from whatever direction from the periphery the pressure point is approached. Relatively strong muscle-fibre curvatures are needed if the distance from the periphery is relatively short (according to equation 2). Smaller curvatures are needed if the distance is relatively long. Hence, in a muscle with a relatively high length to width ratio, the fibre curvatures can be relatively small in the central longitudinal plane, whereas, laterally from the high pressure centre, relatively strong fibre curvatures are required. For the unipennate architecture of figure 8, the high pressure centre will be in the centre of the muscle belly. In this centre, muscle fibres will be (almost) straight (muscle-fibre bundle 5). Owing to the relatively short distance towards the lateral periphery, however, muscle fibres should become strongly curved in this direction (figure 8: fibre bundle 6). These predictions are again supported by dissections (examples are the human mm. soleus and gastrocnemius). Modifications of these considerations are needed if the ambient pressures are quite variable around the muscle belly.

In conclusion, tendinous sheet shape and muscle-fibre shape and arrangement should be tuned relative to each other, so as to meet the demands of (i) mechanical stability, (ii) equality of specific power output and relative length change of the muscle fibres (this demand should not be taken too strict, see text below equation 12), and (iii) an optimal filling of the muscle belly with muscle fibres.

(*c*) *Intramuscular pressure and blood flow*

For the muscle designs of figures 4–7 we calculated maximum intramuscular pressures (using a muscle-fibre stress of 200 kPa for all fibres) in the range of 5.3 to 43.8 kPa. Clearly, the maximum pressure depends on the architecture of the muscle. The highest pressures are likely to be found in muscles with long tendinous sheets, large attachment angles, and strongly curved fibres. The highest calculated pressures were for the relatively long and highly pennated muscle bellies of figures 6*f*, *g* and 7. Somewhat higher pressures may arise for even more extreme architectures in combination with slightly higher muscle-fibre stresses, giving a global maximum for muscle pressure in the order of about 60 kPa. It seems likely that the maximum pressure will only in exceptional cases be higher than about 0.3 times the maximum fibre stress. Further simulations and measurements are needed to clarify this point.

Pressure measurement in muscle tissue is difficult since the introduction of a pressure transducer tends to create a high pressure centre. For cardiac muscle, Gregg & Eckstein (1941) reported a direct relationship between sensor volume and the recorded pressure magnitude. Petrovsky & Hendershot (1984) measured intramuscular pressures in cat leg muscles, by inserting a small rubber balloon into the muscle belly. The balloon was connected to a pressure transducer via a 25-gauge needle. The maximum values of the pressures were about 23 kPa for medial gastrocnemius and about 18 kPa for soleus. In frog gastrocnemius, Hill (1948) measured pressures in the range of about 13 to 38 kPa. All these values are in the order of magnitude of the pressures calculated in the present paper. For isometric contractions, Petrovsky & Hendershot (1984) measured an almost linear relationship between muscle force and intramuscular pressure. A similar relationship was measured by Mazella (1954). Changes in fibre curvature are expected to be small in isometric contractions. Therefore, the roughly linear relationship would be predicted by our theory (if the distribution of force over the fibres is more or less independent of muscle force).

Otten (1988), referring to unpublished results by Kahabuka & Otten, mentions a maximum pressure of 133 kPa for a supramaximally stimulated gastrocnemius muscle (3.4 g) of the toad. A catheter tip pressure transducer was used with a tip diameter of 1.3 mm. Although catheter tip transducers are quite useful for pressure measurement in biological fluid flows (see, for example, Van Leeuwen & Muller 1983), they are unsuitable for hydrostatic pressure measurement in fibrous tissues like a muscle. Distorted

PHILOSOPHICAL TRANSACTIONS OF THE ROYAL SOCIETY B BIOLOGICAL SCIENCES

fibres with 'unnatural' curvatures are likely to be in direct contact with the sensitive membrane so that a too high pressure will generally be recorded. The effect of direct fibre contact is likely to be smaller (but not absent) with the (smoother) balloon.

Pressure measurement may be substantially improved by usage of a servo-nulling transducer (Widerhielm *et al.* 1964). Here, a micropipette (typical tip size in the range of 0.5 to 10 μm) in introduced in the biological tissue. Fluid flow through the pipette is minimized by a servosystem. This technique has been successfully applied in the measurement of intramyocardial pressure (Heineman & Grayson 1985). Intramuscular pressure was found to be lowest at the periphery, whereas it increases towards the cardiac lumen. This is expected from the concentric layers of curved muscle fibres in the cardiac wall (see Arts *et al.* (1991) and references therein). The application of the micropipette technique to skeletal muscle seems to be a promising way to test the present pressure predictions.

Could the muscular pressure cause problems for the blood flow through the muscle? For comparison, the pressure in the aorta of a dog was measured to fluctuate around 14 kPa (Caro *et al.* 1978), considerably below some of the measured and calculated peak intramuscular pressures. Mean blood pressure is reduced by only about 10% before it enters the arterioles, but is reduced to about 4.5 kPa (Charm & Kurland 1974) when it enters the capillaries. The pressure calculations indicate that blood may be squeezed out of the muscle during activation, especially near the high pressure centre (both forwards and backwards). During rhythmic activation, this may actually assist blood flow, since most blood will be expelled into the venous system owing to its lower resistance (and the presence of valves) than that of the arterial system. During prolonged production of a high enough muscle force, however, (as during muscle cramp and spasms) a high muscle pressure may cause ischemia and may limit the endurance. Our model may be helpful to predict which spots in which muscles are most susceptible for ischemia. These viewpoints on muscular blood flow are supported by many well documented experimental studies (e.g. Barcroft & Millen 1939; Lind *et al.* 1964; Petrovsky & Hendershot 1984). Interestingly, Petrovsky & Hendershot (1984) could restore blood flow in (sub)maximally activated gastrocnemius and soleus muscles by increasing artificially the perfusion pressure to 39.9 kPa. As a consequence, the endurance was improved significantly. These experimental studies show also that, at low (isometric) muscle forces (up to about 0.1 of the maximum isometric force) and pressures, blood flow is increased compared to the relaxed state. This is probably due to changes in the cardiovascular system.

(*d*) *Future developments*

The present model can be developed further in several directions. We list a few possibilities below.

1. Using the principles outlined in this paper, other architectures may be studied. Presently, we investigate unipennate architectures.

2. The model may be expanded to three-dimensional architectures, including a variable curvature along the muscle fibres. This could be especially rewarding in a study of the optimal packing of muscle fibres in a muscle belly.

3. The contribution of the endo- and perimysium could be added. This would be useful in a study of muscle shape during (passive) stretch.

4. The model may be expanded to study shape changes of a muscle-tendon complex under dynamic circumstances, including elastic effects of the tendinous sheets. The model of a unipennate muscle with curved muscle fibres and tendinous sheets by Otten (1988) that was claimed to predict shape changes is erroneous (see § 1). Other models are restricted to straight muscle fibres and straight tendinous sheets, with the physical inaccuracies outlined in § 1. Nevertheless, these models have proved to be useful in the prediction of the muscle-force output and power flow among various parts of a muscle-tendon complex (see Zajac 1989; Van Leeuwen 1992).

7. CONCLUSIONS

1. Calculation of mechanically stable muscle architectures, with curved muscle fibres and curved tendinous sheets, is possible with the present model. The internal pressure distribution is calculated from curved muscle fibres under tension. The key to the prediction of muscle shapes is given in equation (7), obtained by equating the pressure from the muscle fibres to the pressure under a curved tendinous sheet under tension. To our knowledge, previous models of muscle architecture are unstable and therefore not capable of predicting muscle shapes (in spite of their usefulness in predicting muscle forces as a function of muscle length; cf. Otten 1988; Zajac 1989; Spoor *et al.* 1991; Van Leeuwen 1992).

2. On a microcomputer, numerical implementations of the present model were made for bipennate and unipennate models. Simulations were made only for two-dimensional architectures. The principles are, however, applicable to a wide variety of muscle architectures, including three-dimensional shapes.

3. In a muscle belly, tendinous sheet shape and muscle-fibre shape and arrangement should be tuned relative to each other, so as to meet the demands of (i) mechanical stability, (ii) equality of specific power output and relative length change of the muscle fibres (this demand should not be taken too strict, see § 4), and (iii) an optimal filling of the muscle belly with muscle fibres. The latter demand was unsufficiently met in the bipennate two-dimensional models. It is discussed how this problem can be solved in a special three-dimensional arrangement of the muscle fibres, in combination with varying widths of the tendinous sheets.

4. The maximum intramuscular pressure generated depends on the maximum tensile muscle-fibre stress, and shape characteristics like muscle-fibre attachment angles, but not on the size of the muscle. The highest

PHILOSOPHICAL TRANSACTIONS OF THE ROYAL SOCIETY B BIOLOGICAL SCIENCES

pressures are likely to be found in muscles with long tendinous sheets, large attachment angles, and strongly curved fibres. Higher internal pressure values may be found if muscles are covered by other curved muscles.

5. Intramuscular pressures can be high enough (up to 43.8 kPa in the simulation of figure 7) to obstruct blood flow. Therefore, cramps and spasms may lead to ischemic circumstances in muscles. Repetitive muscle activation, however, may assist the circulation. The present model may be an important aid in the location of high pressure centres in muscles.

We thank Dr M. R. Drost for a useful discussion about biological pressure measurement. Professor R. McNeill Alexander and Dr M. Muller are thanked for valuable comments on a draft of this paper.

REFERENCES

Akster, H.A. 1981 Ultrastructure of muscle fibres in the head and axial muscles of the perch (*Perca fluviatilis* L.). A quantitative study. *Cell. Tiss. Res.* **219**, 111–131.

Alexander, R.McN. 1983 *Animal mechanics*. Oxford: Blackwell Scientific Publications.

Alexander, R.McN. 1969 The orientation of muscle fibres in the myomeres of fishes. *J. mar. biol. Ass. U.K.* **49**, 263–289.

Arts, T., Bovendeerd, P.H.M., Prinzen, F.W. & Reneman, R.S. 1991 Relation between left ventricular cavity pressure and volume and systolic fiber stress and strain in the wall. *Biophys. J.* **59**, 93–102.

Barcroft, H. & Millen, J.L.E. 1939 The blood flow through muscle during sustained contraction. *J. Physiol., Lond.* **97**, 17–31.

Benninghoff, A. & Rollhäuser, H. 1952 Zur inneren Mechanik des gefiederten Muskels. *Pflügers Arch. ges. Physiol.* **254**, 527–548.

Caro, C.G., Pedley, T.J., Schroter, R.C. & Seed, W.A. 1978 *The mechanics of the circulation*. Oxford University Press.

Charm, S.E. & Kurland, G.S. 1974 *Blood flow and microcirculation*. New York: Wiley & Sons.

Gregg, D.E. & Eckstein, R.W. 1941 Measurements of intramyocardial pressure. *Am. J. Physiol.* **132**, 781–790.

Gans, C. & Bock, W.J. 1965 The functional significance of muscle architecture—a theoretical analysis. *Ergebn. Anat. Entw. Gesch.* **38**, 115–142.

Haughton, S. 1873 *Principles of animal mechanics*. London: Longmans, Green and Co.

Heineman, F.W. & Grayson, J. 1985 Transmural pressure of intramyocardial pressure measured by micropipette technique. *Am. J. Physiol.* **249**, H1216–1223.

Hill, A.V. 1948 The pressure developed in muscle during contraction. *J. Physiol., Lond.* **107**, 518–526.

Huijing, P.A. & Woittiez, R.D. 1984 The effect of architecture on skeletal muscle performance: A simple planimetric model. *Neth. J. Zool.* **34**, 21–32.

Lind, A.R., Taylor, S.H., Humphreys, P.W., Kennelly, B.M. & Donald, K.W. 1964 The circulatory effects of sustained voluntary muscle contraction. *Clin. Sci.* **27**, 229–244.

Mazella, H. 1954 On the pressure developed by the contraction of striated muscle and its influence on muscular circulation. *Arch. Int. Physiol.* **62**, 334–347.

Otten, E. 1985 Some numerical reflections upon a simple planimetric muscle model of Huijing and Woittiez. *Neth. J. Zool.* **35**, 517–520.

Otten, E. 1988 Concepts and models of functional architecture in skeletal muscle. In *Exercise Sport Sci. Rev.*, vol. 16 (ed. K. B. Pandolf), pp. 89–139. New York: MacMillan.

Petrovsky, J.S. & Hendershot, D.M. 1984 The interrelationship between blood pressure, intramuscular pressure, and isometric endurance in fast and slow twitch skeletal muscle in the cat. *Eur. J. appl. Physiol.* **53**, 106–111.

Purslow, P.P. 1989 Strain-induced reorientation of an intramuscular connective tissue network: implications for passive muscle elasticity. *J. Biomechan.* **22**, 21–31.

Spoor, C.W., Van Leeuwen, J.L., De Windt, F.H.J. & Huson, A. 1989 A model study of muscle forces and joint-force direction in normal and dysplastic neonatal hips. *J. Biomechan.* **22**, 873–884.

Spoor, C.W., Van Leeuwen, J.L., Van der Meulen, W.J.T.M. & Huson, A. 1991 Active force-length relationship of human lower leg muscles estimated from morphological data: A comparison of geometric muscle models. *Eur. J. Morph.* **29,** 137–160.

Stenonis, N. (Stensen, N.) 1667 *Elementorum Myologiæ Specimen, seu Musculi Descriptio Geometrica*, vol 2, pp. 61–111. Florence: Stellae.

Van Leeuwen, J.L. 1991 Optimum power output and structural design of sarcomeres. *J. theor. Biol.* **149**, 229–256.

Van Leeuwen, J.L. 1992 Muscle function in locomotion. In *Mechanics of animal locomotion* (ed. R.McN. Alexander), pp. 191–250. Heidelberg: Springer-Verlag.

Van Leeuwen, J.L. & Muller, M. 1983 The recording and interpretation of pressures in prey-sucking fish. *Neth. J. Zool.* **33**, 425–474.

Wickiewicz, T.L., Roy, R.R., Powel, P.L. & Edgerton, V.R. 1983 Muscle architecture of the human lower limb. *Clin. Orthop. Rel. Res.* **179**, 275–283.

Widerhielm, C.A., Woodbury, J.W., Kirk, S. & Rushmer, R.F. 1964 Pulsatile pressures in the microcirculation of the frog's mesentary. *Am. J. Physiol.* **207**, 173–176.

Woittiez, R.D., Huijing, P.A., Boom, H.B.K. & Rozendal, R.H. 1984 A three-dimensional model: A quantified relation between form and function of skeletal muscles. *J. Morphol.* **182**, 95–113.

Zajac, F.E. 1989 Muscle and tendon: properties, models, scaling, and application to biomechanics and motor control. In *CRC critical reviews in biomedical engineering* (ed. J.R. Bourne), vol 17, pp 359–411. Baco Raton: CRC Press.

Received 2 December 1991; accepted 10 December 1991

PHILOSOPHICAL TRANSACTIONS OF THE ROYAL SOCIETY B BIOLOGICAL SCIENCES

(*a*) Human medial gastrocnemius muscle

(*b*) Muscle fibre arrangement in simulated muscle belly

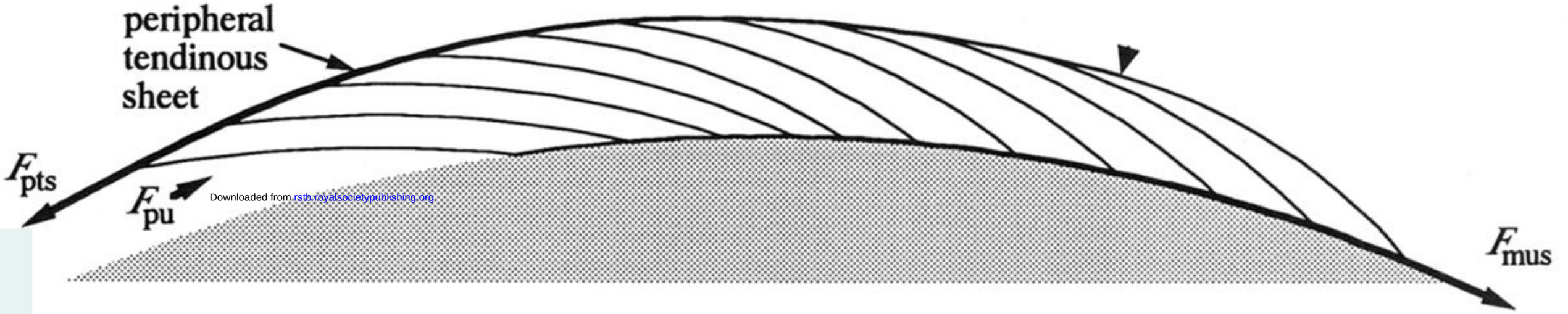

(*c*) Pressure contours (fraction of maximum pressure)

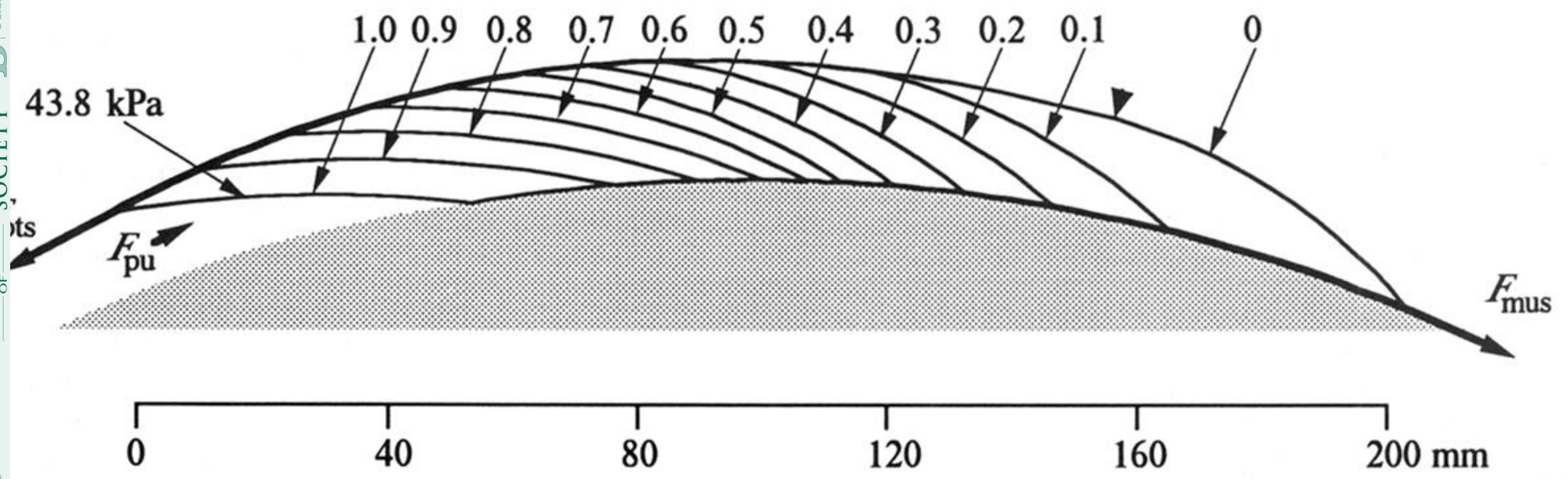

gure 7. Comparison between human medial gastrocnemius and unipennate simulation. (*a*) Dissected gastrocne-ius so as to expose the central longitudinal plane. (*b*) Muscle-fibre arrangement of simulation of mechanically able unipennate muscle belly. (*c*) Intramuscular pressure contours as a fraction of the maximum pressure 3.8 kPa) of the same simulation. The shaded areas in (*b*) and (*c*) depict the boundary against which the muscle lly presses. Arrow heads point to the transitions between tendinous sheet and peripheral muscle fibre. The scale fers to all illustrations. Some parameter values are as follows (per unit width where applicable): $c_{fb} = 5.10\ m^{-1}$; $= 4.23\ m^{-1}$; curvature of lower sheet $= 3.57\ m^{-1}$; $\beta_{fb} = 18.5°$; $\sigma_f = 200$ kPa; $u = 0.85$; $V_{mus} = 2909.2\ mm^2$; $V^*_{fib} = 0.601$; $_{ib} = 28.71$ mm; $l_{pts} = 166.0$ mm; $F_{mus} = 5201.5\ mN\ mm^{-1}$; $F_{pts} = 5587.5\ mN\ mm^{-1}$; $p_{max} = 43.79$ kPa; $p^*_{max} = 0.219$. he contribution of the transverse tensile stress along the upper sheet to the internal pressure, p_{trq}, was defined to ıry linearly from 0% of the muscle-fibre pressure (equation 3) at the left side to 20% at the right side. See § 2 for mbols. Further explanation in the text.